ELSEVIER

Materials Science and Engineering B 140 (2007) 73–80

MATERIALS SCIENCE & ENGINEERING B

www.elsevier.com/locate/mseb

Gas sensing behavior of nanostructured sensors based on tin oxide synthesized with different methods

M.R. Vaezi *, S.K. Sadrnezhaad

Advanced Materials Research Center, Materials and Energy Research Center, Karaj, Iran

Received 14 January 2007; received in revised form 26 March 2007; accepted 11 April 2007

Abstract

Tin oxide, SnO_2 nanomaterials fabricated by chemical precipitation (CP), sol–gel (SG), and dissolution pyrolysis (DP) are characterized using X-ray diffraction, scanning electron microscopy and transmission electron microscopy. The gas sensing properties of tin oxide nanomaterials prepared by CP, SG and DP methods have been studied. The results show that tin oxide nanopowders produced from three above-mentioned methods have tetragonal rutile structure and the mean size of particles are less than 30 nm. The results obtained from SEM show that tin oxide thick films (produced from the synthesized nanopowders) coated onto alumina substrates have different morphology and tin oxide thick films fabricated through DP method has porous structure. By the results obtained from the gas sensing behavior, the gas sensor based on tin oxide prepared by DP method has high sensitivity, excellent selectivity, quick response and recovery behavior to gases investigated compared with those fabricated by the other two methods.
© 2007 Elsevier B.V. All rights reserved.

Keywords: Nanomaterial; Chemical precipitation; Sol–gel; Dissolution pyrolysis; Tin oxide; Gas sensing behavior

1. Introduction

Efforts towards the development of simple, inexpensive and reliable devices have recently been increased with the aim to control air pollution and to detect toxic or smelling gases at low levels in the air and in the field of domestic and industry applications. Semiconducting oxides such as tin oxide, zinc oxide, titanium oxide and so on are widely used as sensing materials due to their surface properties involved in the reaction mechanism with the gas to be detected [1–5]. As we all know, tin oxide is currently used for a wide range applications including gas sensors, catalysts and electrochemical and photo-electrochemical based energy conversions [6–11]. Sensitivity has been shown to be enhanced when the tin oxide grain diameter is on the order of the thickness of the charge depletion layer, approximately 6 nm [12,13]. There are numerous methods for the preparation of tin oxide nano-particles [14,15] and films, such as sputtering [16,17], sol–gel [18,19], chemical vapor deposition (CVD) [20], sonochemical processing [21–23] and thermal evaporation [24].

In this research work, we fabricated gas sensors based on tin oxide prepared by chemical precipitation, sol–gel and dissolution pyrolysis and the gas sensitive properties to various gases such as Cl_2, NO_2, gasoline and ethanol were discussed.

2. Experimental

2.1. Preparation of tin oxide nanopowders

2.1.1. CP method

"Extra pure" $SnCl_4{\cdot}5H_2O$ of 98% purity (Sigma–Aldrich, 14550) was used as precursor. A supply of 0.1 M solution of $SnCl_4$ in deionized water was prepared. With stirring the solution, concentrated ammonia was dropped in it until pH was greater than 8. The obtained precipitates were washed with the deionized water several times and then dried at 100 °C in oven for 24 h. The powders were annealed at 650 °C for 6 h. The powder prepared via chemical precipitation is termed as CP.

2.1.2. SG method

Five hundred cubic centimeters of 0.1 M solution of $SnCl_4$ in deionized water was prepared. Fifty cubic centimeters of concentrated citric acid was dropped into the solution stirring all the times until the citric acid dissolved. Then concentrated ammo-

* Corresponding author.
E-mail addresses: vaezi9016@yahoo.com (M.R. Vaezi), sadrnezh@sharif.edu (S.K. Sadrnezhaad).

0921-5107/$ – see front matter © 2007 Elsevier B.V. All rights reserved.
doi:10.1016/j.mseb.2007.04.011

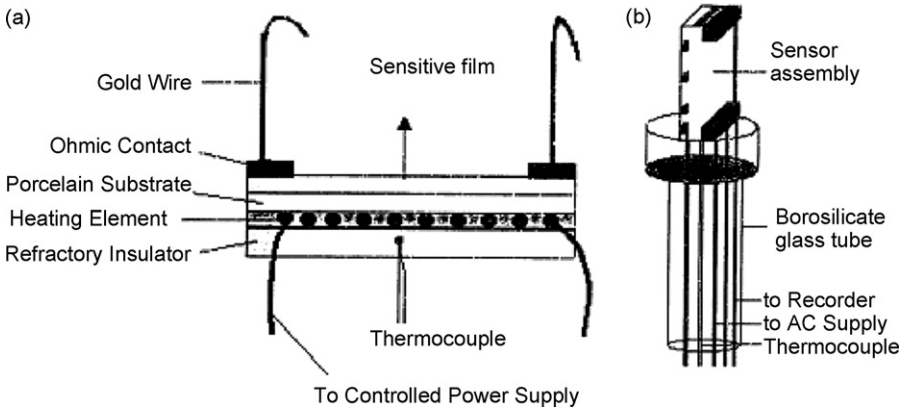

Fig. 1. Schematic illustrations of the fabricated gas sensor (a) and the sensor probe (b).

nia was dropped in it until pH was greater than 8. After stirring the mixture, sol is formed. The formed sol was evaporated on the water bath at 80 °C and then dried at 100 °C in oven for 24 h until xerogel formed. The xerogel was pre-annealed at 200 °C for 2 h. Finally, the pre-annealed xerogel annealed at 650 °C for 6 h. The powder prepared via sol–gel method is termed as SG.

A certain amount of metallic tin was mixed with citric acid (1:30 wt%) and some water. The mixture was stirred till the citric acid was dissolved completely. Then it is stirred at 180 °C for 48 h. The subsequent stages were the same as xerogel in Section 2.1.2. The powder prepared via dissolution pyrolysis method is termed as DP.

SnO_2 thick films produced in this work were characterized for their surface morphology, size and the shape of particles, phases present and preferred orientation. The surface morphology was studied by scanning electron microscopy (SEM) using a Philips model MV2300 operated at 25 kV. X-ray diffraction (XRD) was used to determine the phase present and the preferred orientation of the deposits. A Philips Xpert-Pro X-ray diffractometer with a Cu Kα radiation (λ = 1.5418 Å) was employed to obtain XRD spectra using standard θ–2θ geometry. A computer-based search and match was used for phase identification. The size and the shape of particles were analyzed by TEM.

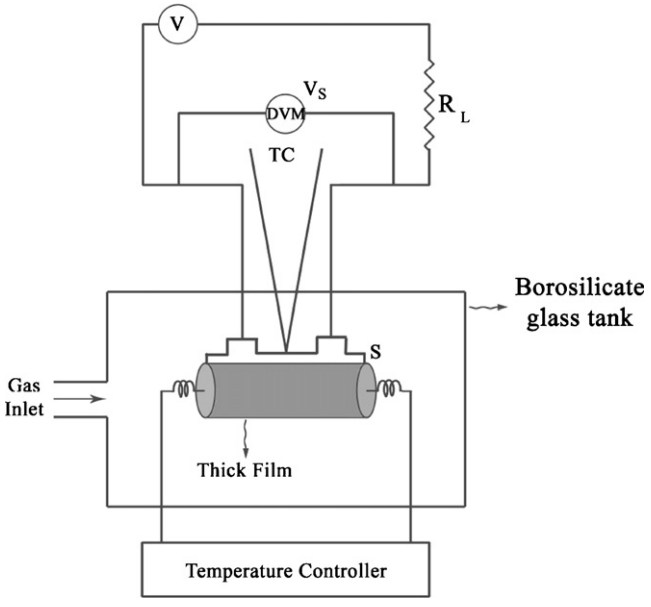

Fig. 2. Schematic of the set up used for measuring the change in resistance on exposure to gases. *V*, supply voltage; *S*, sensor probe; DVM, digital voltmeter.

2.2. Sensor fabrication and measurements

Twenty cubic centimeters of α-terpineol was added to the obtained powders and then the mixture was ground to form paste. The paste obtained was coated (thick film fabrication method) onto alumina plate as the substrate. The metallization was carried out by paste printing of a high temperature conductive epoxy resin (Duralco-124). Two electrodes of 2 mm × 4 mm were deposited on each device. Thin gold wires were cemented to the metallized area by the same epoxy. The sample was then gradually heated up to 200 °C for epoxy curing and contact stabilization. The metal contacts were tested to be ohmic. The substrate was then attached to a temperature-controlled micro-heater, and was mounted on a refractory stand, so that the temperature of the substrate could be adjusted in the 25–450 °C temperature range. The structure of the device is schematically presented in Fig. 1a. A sensor probe was formed by mounting the sample on a thick-walled borosilicate glass tubing, through which two insulated connection cables were guided to the temperature control unit and the impedance measurement device, respectively, Fig. 1b. For each sensitivity measurement, the sen-

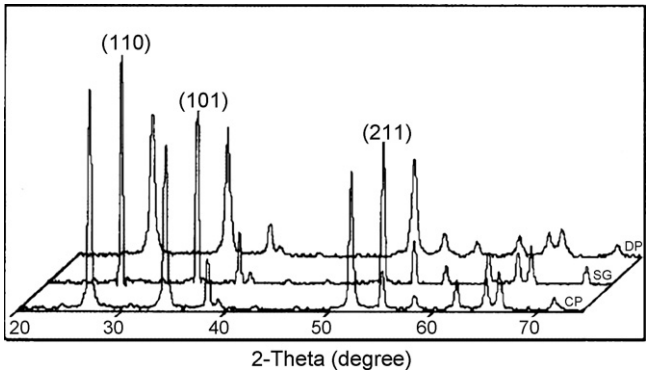

Fig. 3. XRD patterns of samples CP, SG and DP.

sor probe was set at the desired operating temperature (see below) and a 10 min time was allowed for the probe temperature to stabilize. A load resistor, R_L was connected in series with the sensor element, R_S. Then, a constant AC voltage (10 V, 80 Hz) was applied across R_L and R_S. DC fields could cause ionic migration and electrode instability which were of much lesser concern in the case of AC voltages applied. Test gases were passed into the borosilicate glass tank. The resistance of the sensor was obtained by measuring the voltage drop, V_S across the sensor element. A chromel–alumel thermocouple

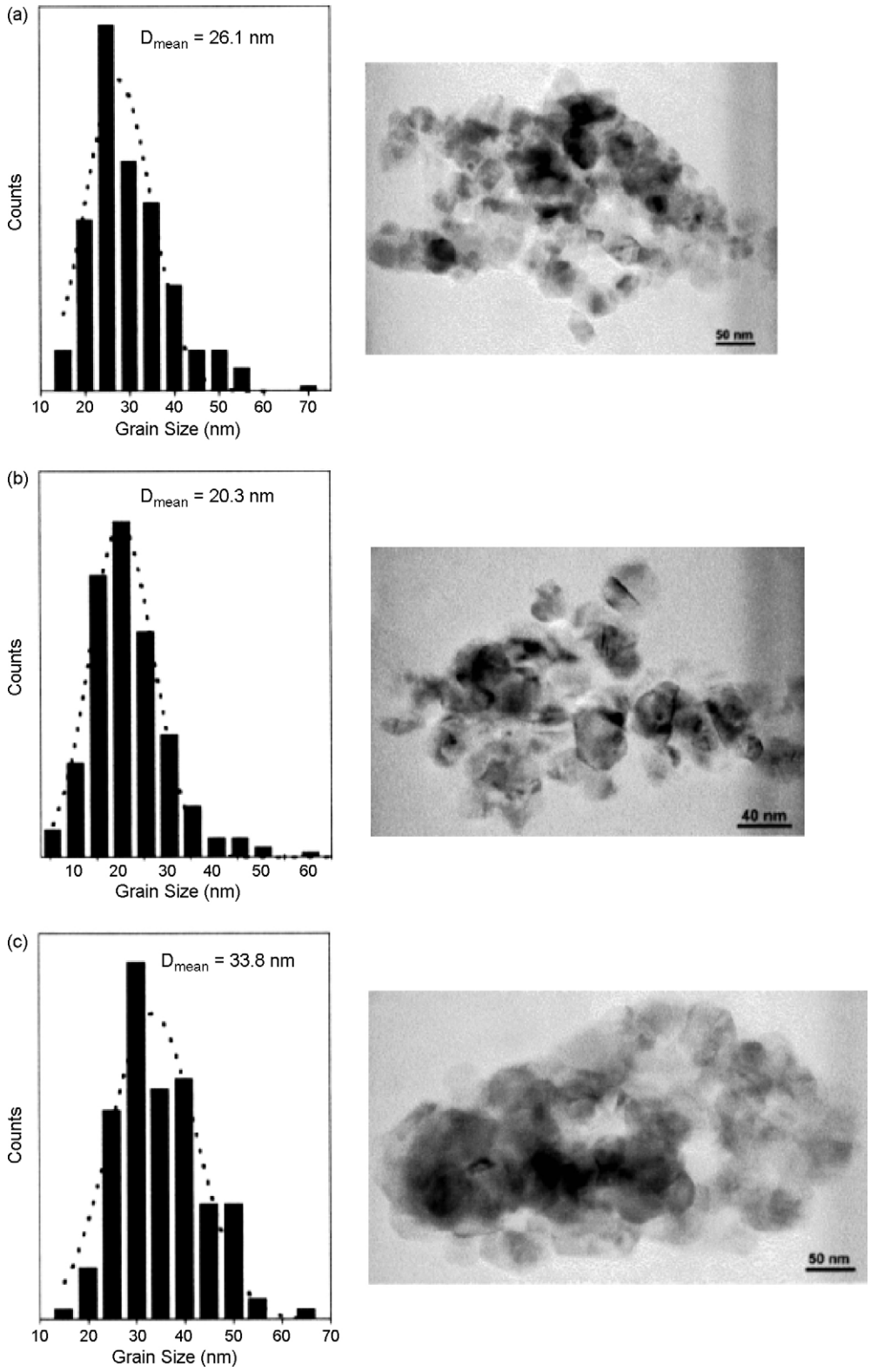

Fig. 4. TEM images of samples: CP (a), SG (b) and DP (c).

(TC) was placed on the device to indicate the operating temperature. The schematic of the measurement set up is shown in Fig. 2. To avoid errors cause by condensation of the contaminating gas on the walls of the tank, it was externally heated up to 50 °C.

Different definitions of the sensitivity of a gas sensor to a particular target gas have been presented in the background literature [25–27]. In this paper, the sensitivity of sensor, S, is defined as $S = R_g/R_a$, in which R_g and R_a are the steady state resistances of the sensor in gas contaminated air and pure air, respectively. According to this definition, R_g and R_a should both be measured at the operating temperature of the device.

3. Results and discussions

3.1. Characterization of the samples

XRD patterns of tin oxide powders prepared by three methods are shown in Fig. 3. All the diffraction peaks can be indexed to the tetragonal rutile structure of SnO_2 with lattice constants of $a = 4.741$ Å and $c = 3.191$ Å, $a = 4.739$ Å and $c = 3.19$ Å, $a = 4.74$ Å and $c = 3.188$ Å of CP, SG and DP samples, respectively. From the XRD patterns, we can know that the crystallite sizes of CP, SG and DP samples are about 21, 23 and 25 nm, respectively. These values were calculated from the Scherrer formula.

In Fig. 4, the typical grain size histograms of the tin oxide nanopowders synthesized by different methods are shown together with their TEM grain images. It is shown that the samples are spherical particles with quite uniform grain size distribution. The average grain diameters of samples CP, SG and DP are 26.1, 20.3 and 33.8 nm, respectively. As we can see, the results obtained from TEM images correspond with a little different to those calculated by Scherrer formula according to XRD patterns. This little difference between XRD and TEM results seems within the acceptable range of errors possibly existing in our measurements.

Fig. 5 shows the microstructures of tin oxide thick films prepared from CP, SG and DP methods. As is shown in the figure, the thick films prepared from the above-mentioned methods have different microstructures. The SEM images show that the surface of DP, SG and CP samples is composed of porous, smooth surface containing some dot marks and cracks, respectively. The dot marks of SG sample were formed by impurity via energy dispersive spectrometer (EDS) (Fig. 6). EDS spectrum of tin oxide thick film prepared by SG method, SG sample, shows the presence of Sn, O, Al and a trace amount of Cl. The source of Al is the substrate. The Cl species may have come from the solution.

3.2. Gas sensing behavior

S is temperature dependent, and tin oxide based gas sensors are operated at elevated temperatures. S increases with temperature as the interaction at the gas–solid interface is accordingly enhanced. However, at a certain temperature the thermal carrier generation mechanism over shadows the same caused by the interaction with the target gas. Also the thermal deposition of the target gas molecules from the sensitive surface at

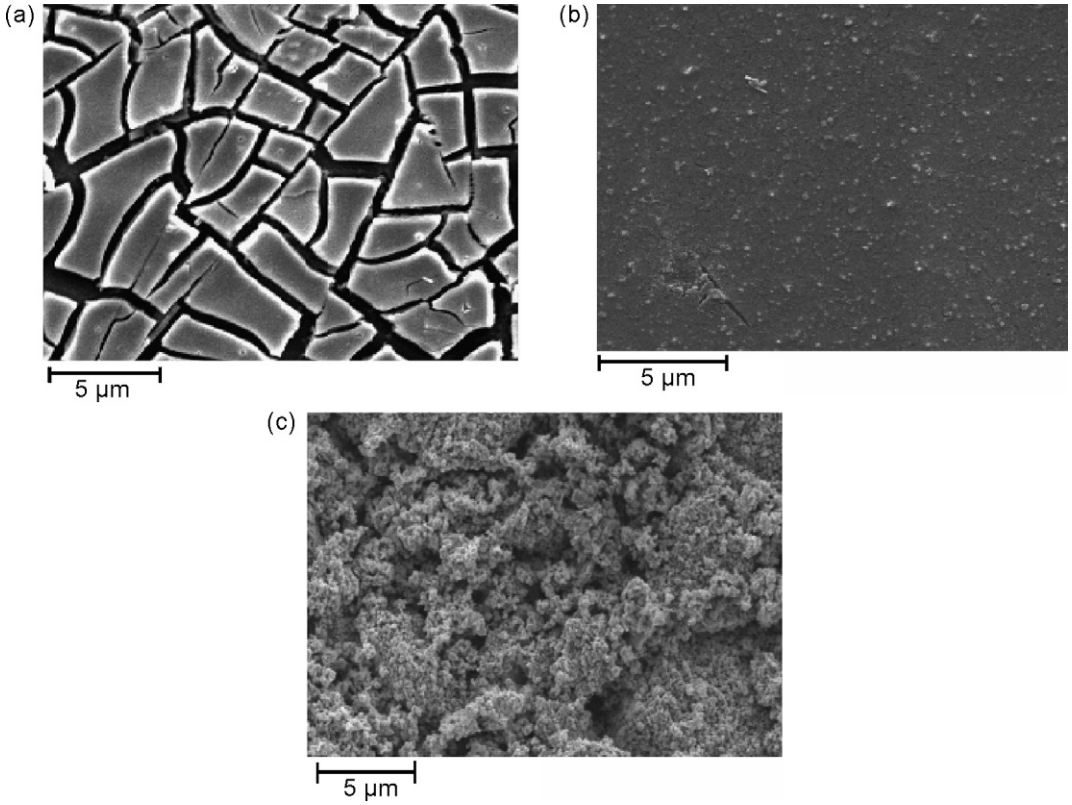

Fig. 5. SEM images of the surface of tin oxide thin film prepared from CP (a), SG (b) and DP (c) method.

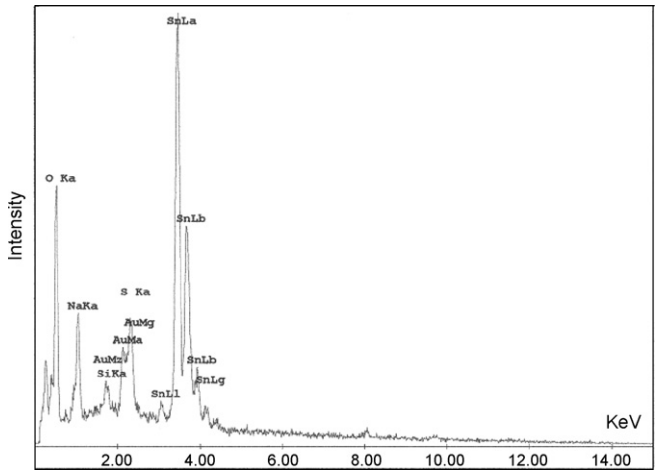

Fig. 6. EDS result of SG sample.

higher temperatures becomes more significant and hinders the solid–gas interaction required for carrier generation [28]. Hence, it is important to find the maximum sensitivity temperature for the sample devices fabricated. In Fig. 7 the results of our sensitivity measurements at various operating temperatures, 25–400 °C, are presented. In these experiments, the target gases were Cl_2, NO_2, gasoline and ethanol at a concentration of 50 ppm. It was concluded from Fig. 7a and d that the sensor prepared by DP method had the maximum sensitivity to ethanol ($S = 476$), and Cl_2 ($S = 225$), at 350 °C. As it was shown in Fig. 7a and b, the sensitivity of the sensor prepared by DP method to Cl_2 and NO_2 were 30 and 45 at 25 °C, respectively, but the sensor prepared by CP and SG method had no sensitivity to gases at 25 °C. Also, the sensor prepared by DP method has higher sensitivity to Cl_2, NO_2, gasoline and ethanol than the sensors prepared by CP and SG method. For example, the maximum sensitivity of the sensors prepared by CP, SG and DP method to Cl_2 gas are 45, 35 and 225, respectively. Because of high sensitivity and easy preparation of the sensors prepared by DP method, it could easily be put into practical use.

The adsorption/desorption processes occurred on the surface of the semiconductors such as tin oxide can determine the changes of surface potential and the gas sensing properties of metal oxide films [29–31]. The species of H_2O, OH, O_2 and O are the main agents which can be adsorped on the surface [29]. The temperature ranges within which these surface species exist at the surface are determined by their energies of desorption which correspond to the following order [32]:

$$H_2O < O_2 < OH < O$$

Desorption of H_2O begins at the temperatures more than 30–50 °C. Therefore, it is concluded that at the temperatures more than 80 °C the influence of molecular water is negligible [30]. Desorption of O_2 takes place at $T > 50$ °C. At $T > 200$–250 °C the presence of molecular oxygen on the surface of tin oxide is also negligible [33]. According to the literatures [29,34], the chemisorbed atomic oxygen is not observed at room temperature on the surface of undoped tin oxide. Atomic oxygen appears on the tin oxide surface at $T \approx 180$ °C. At $T > 200$ °C this form of oxygen becomes dominant on the surface of tin oxide. When the molecular oxygen is adsorbed on the surface of tin oxide, it traps electron(s) from the body of tin oxide due to the strong electronegativity of the oxygen atom to produce

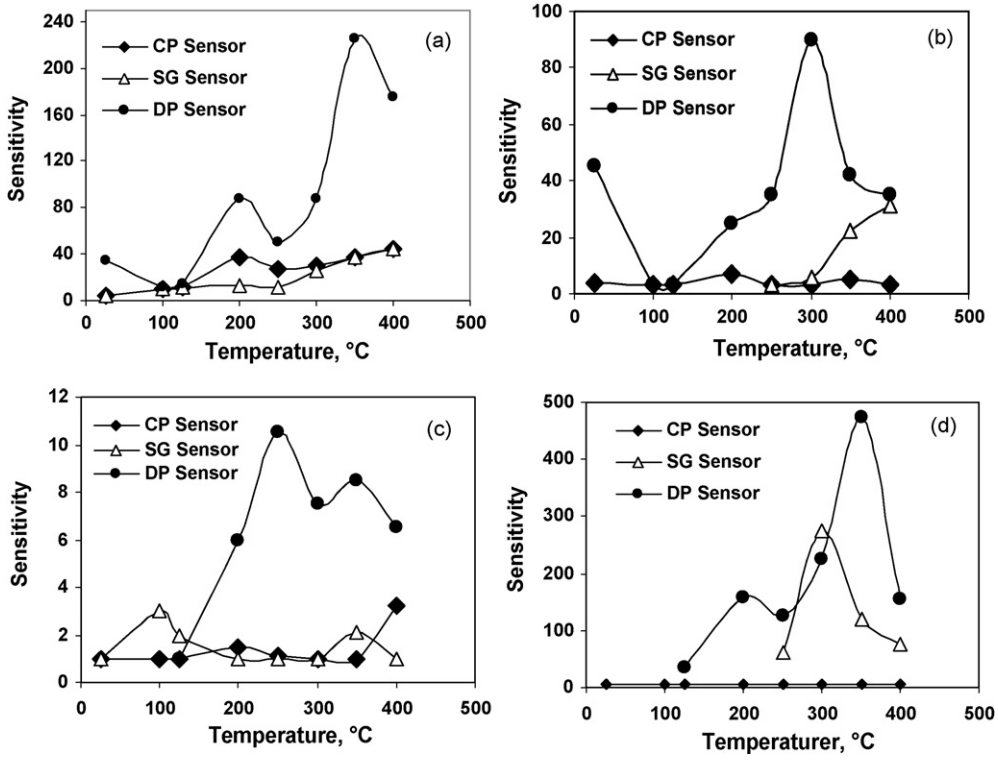

Fig. 7. The experimental relationship between the sensitivity to 50 ppm Cl_2 (a), NO_2 (b), gasoline (c) and ethanol (d) in the gas sensors fabricated.

negatively charged and chemisorbed oxygen such as O_2^-, O^- and O^{2-}. Then the concentration of electrons in the tin oxide decreases and hence the resistance of the material increases.

When the surface of material exposed to the reducing gas, the interaction with the chemisorbed oxygen can take place in various ways. For example, these surface reactions can be written for the ethanol as the following [34]:

$$C_2H_5OH + O_2 \rightarrow CH_3CHO + H_2O$$

$$CH_3CHO + O^- (ads.) \rightarrow CO_2 + H_2O + e$$

While the surface of the sensor material exposed to the oxide gases, such as NO_2, it can be adsorbed or interact with the oxygen adsorbed onto the sensor material according to the following reactions [35]:

$$NO_2 (gas) + e \rightarrow NO_2^-$$

$$NO_2 (gas) + O_2^- + 2e \rightarrow NO_2^- + 2O^-$$

Two type of atomic oxygen, O_2^- and O^-, are dominant species on the surface of tin oxide at $T > 200\,^\circ C$ and these forms of atomic oxygen have the main effect on the reaction of tested gases. So the highest sensitivity appeared at $T > 200\,^\circ C$. We all know that Cl_2 is more active than NO_2 on the surface of tin oxide. Therefore, Cl_2 reacts with chemisorbed oxygen more easily than NO_2 and the sensitivity of CP, SG and DP sensors to Cl_2 is higher than those to NO_2. Also, ethanol, reducing gas, can react with oxygen more easily than oxidizing gases. So, the sensitivity of SG and DP sensor to ethanol is higher than oxidizing gases.

Shukla and Seal [36] proposed that gas sensitivity of nanocrystalline tin oxide increases with decreasing the particle size. When the particle size decreases, the surface to volume ratio increases largely which leads to better sensitivity. In this research work, we combined the analysis of XRD patterns (Fig. 3) with the TEM images (Fig. 4) and obtain that particles size of CP, SG and DP samples are all small but their sensitivities are different. From SEM images of these samples (Fig. 5) we obtained that the surface of DP sample was porous structure, while there were dot marks on the smooth surface of SG sample and cracks on the surface of CP sample. The porous structure of DP sample cause to increase the interactions between gas and the surface of material and therefore improve the gas sensitivity. The dot marks and the smooth surface of SG sample will decrease the interaction of the gases with material. Also, the cracks in the morphology of CP sample increase the resistance of the sensor. It is concluded that the sensitivity of sensors fabricated would be influenced by their microstructure.

Selectivity is another important characteristic of gas sensors. Theoretically, the sensors should have high sensitivity to some gases and little or no sensitivity to other gases in the same surroundings. The sensitivity of CP, SG and DP sensors to four gases is measured at a concentration of 50 ppm. The optimal working temperature of these sensors is 210, 300 and 350 °C, respectively. In Fig. 8, the results of these measurements are presented. It can be shown that the DP sensor has a good selectivity to ethanol versus gasoline at 350 °C. Also, the selectivity of DP sensor is higher than SG sensor. Therefore, we can detect ethanol easily in the mixture of ethanol and gasoline. Incidentally, it is significant to discuss the selectivity of sensors to Cl_2 versus NO_2. As it is shown from Fig. 8, the CP and DP sensors have the selectivity of Cl_2 versus NO_2 and the selectivity of DP sensor is higher than CP sensor. Therefore, the DP sen-

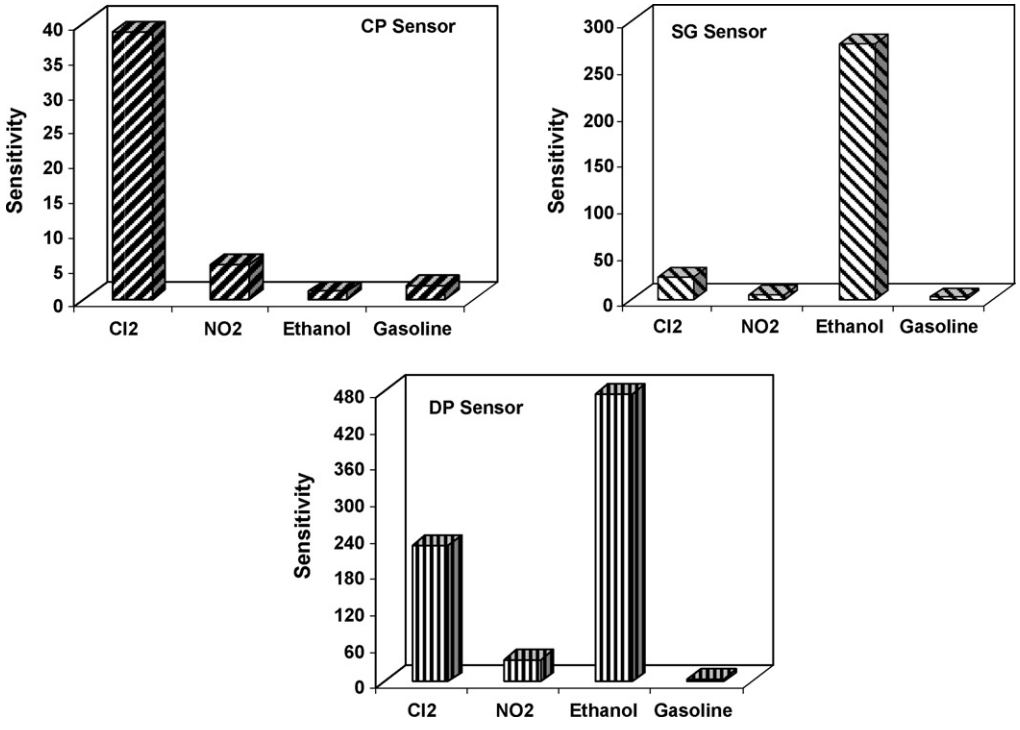

Fig. 8. Selectivity of CP, SG and DP sensors to various gases at optimum working temperature.

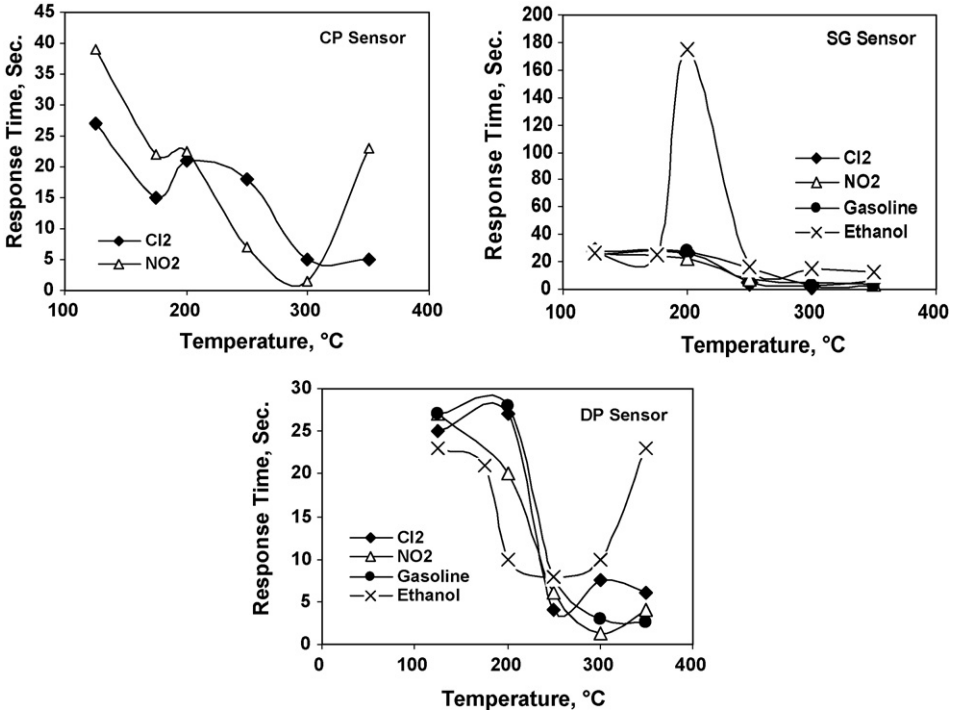

Fig. 9. Response time of CP, SG and DP sensors towards 50 ppm various gases.

sor has good selectivity to ethanol and Cl_2. It is concluded that the sensors based on tin oxide prepared by DP method have the sensitivity either oxidizing gases or reducing gases and their selectivity to ethanol and Cl_2 is satisfactory. So, we can conclude that the DP sensor has better sensing properties than CP and SG sensor.

Fig. 9 shows the response time as a function of the operating temperature for SG and DP sensors towards 50 ppm Cl_2, NO_2, gasoline and ethanol as well as CP sensor towards 50 ppm Cl_2 and NO_2. Because of low sensitivity of CP sensor to gasoline and ethanol, its response and recovery times has been studied. For the examined gas sensors, the response time decreases with

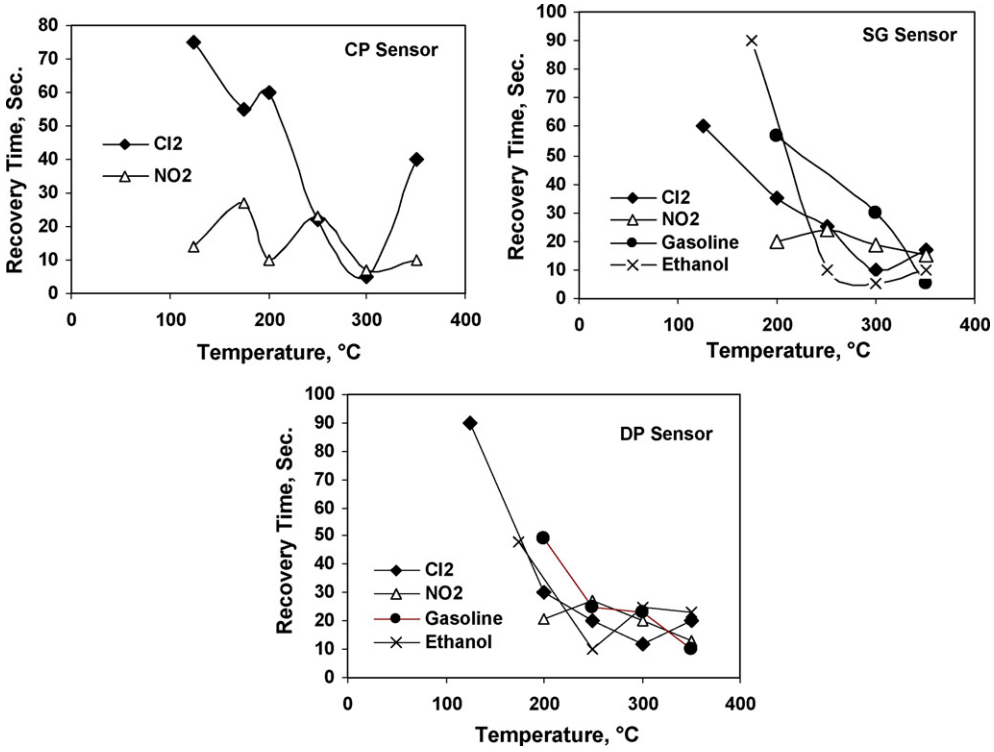

Fig. 10. Recovery time of CP, SG and DP sensors towards 50 ppm various gases.

the temperature. The higher speed of response of SG and DP sensors to Cl_2, NO_2 and gasoline than ethanol is shown. At 350 and 300 °C, the response time of SG and DP towards Cl_2 and NO_2 is very short. For example, 4 and 3 s towards 50 ppm NO_2 at 350 °C for DP and SG sensor, respectively, against 23 s for CP sensor. At 250 °C, the DP sensor still has short response time to Cl_2, NO_2, gasoline and ethanol (4, 6, 8 and 9 s, respectively) whereas the response time of CP and SG sensor is longer than 10 s.

Fig. 10 shows the recovery time versus the operating temperature for the SG and DP sensors towards 50 ppm Cl_2, NO_2, gasoline, ethanol and CP sensor towards 50 ppm Cl_2 and NO_2. As it is shown, the recovery time of SG and DP sensors decreases with the temperature and DP sensor shows the higher rate of recovery than SG sensor.

Taking into account the result of sensitivity, response and recovery times, it is concluded that the DP sensor has good sensing properties such as high sensitivity, good selectivity, short response and recovery times and low working temperature.

4. Conclusions

In this paper, the sensor devices based on tin oxide were fabricated by different methods such as chemical precipitation, sol–gel, and dissolution pyrolysis. Tin oxide based sensor fabricated by DP method has porous morphology and contains fine-grain structure. These characteristics improve the sensing properties and therefore this sensor can be considered as a good sensing material. Also, it is concluded that the sensor fabricated by DP method is a promising gas sensor for detecting Cl_2, NO_2 and ethanol with high sensitivity and appropriate selectivity. Furthermore, the sensitivity of the sensor fabricated by DP method to Cl_2 and NO_2 is relatively high at room temperature. Therefore, this method, DP method, will produce the sensors which are useful in practice.

References

[1] T. Maosong, D. Guorui, G. Dingsan, Appl. Surf. Sci. 171 (2001) 226–230.
[2] G. Leo, R. Rella, P. Siciliano, S. Capone, J.C. Alonso, V. Pankov, A. Ortiz, Sens. Actuators B 58 (1999) 370–374.
[3] A. Ahmad, J. Walsh, T.A. Wheat, Sens. Actuators B 93 (2003) 538–545.
[4] G.G. Mandayo, E. Castano, F.J. Gracia, A. Cirera, A. Cornet, J.R. Morante, Sens. Actuators B 95 (2003) 90–96.
[5] E. Comini, G. Faglia, G. Sberveglieri, Sens. Actuators B 76 (2001) 270–274.
[6] P.W. Zhang, R.D. Zu, L.W. Zhong, Science 291 (2001) 1947–1949.
[7] D.F. Zhang, L.D. Sun, J.L. Yin, C.H. Yan, Adv. Mater. 15 (2003) 1022–1025.
[8] Z.R. Dai, J.L. Gole, J.D. Stout, Z.L. Wang, J. Phys. Chem. B 106 (2002) 1274–1279.
[9] A. Kolmakov, Y. Zhang, G. Cheng, M. Moskovits, Adv. Mater. 15 (2003) 997–1000.
[11] Y. Liu, C. Zhang, W. Wang, C. Yin, G. Wang, Adv. Mater. 13 (2001) 1883–1887.
[12] C. Xu, J. Tamaki, N. Miura, N. Yamazoe, Sens. Actuators B 3 (1991) 147–155.
[13] G. Zhang, M. Liu, Sens. Actuators B 69 (2002) 144–152.
[14] P. Ménini, F. Parret, M. Guerrero, K. Soulantica, L. Erades, A. Maisonnat, B. Chaudret, Sens. Actuators B 103 (2004) 111–114.
[15] M.R. Vaezi, S.K. Sadrnezhaad, Mater. Des. 28 (2007) 515–519.
[16] D.J. Rickerby, M.C. Horrillo, J. Nanostruct. Mater. 10 (1998) 357–363.
[17] G. Sberveglieri, G. Faglia, S. Groppelli, P. Nelli, C. Perego, Sens. Actuators B 13 (1993) 117–120.
[18] A. Dieguez, A.R. Rodriguez, J.R. Morante, J. Kappler, N. Barsan, W. Copel, Sens. Actuators B 60 (1999) 125–137.
[19] N.L. Wu, L.F. Wu, Y.C. Yang, S.J. Huang, J. Mater. Res. 14 (1996) 813–820.
[20] P. Rajaram, Y.C. Goswami, S. Rajagopalan, V.K. Gupta, Mater. Lett. 54 (2002) 158–163.
[21] L. Qui, V.G. Pol, J. Calderon-Moreno, A. Gedanken, Ultrasonics Sonochem. 12 (2005) 243–247.
[22] Y. Feng, R. Yao, L. Zhang, Physica B: Condens. Matter 350 (2004) 348–352.
[23] Y.S. Feng, S.M. Zhou, Y. Li, C.C. Li, L.D. Zhang, Solid State Sci. 5 (2003) 729–733.
[24] V.R. Katti, A.K. Debnath, K.P. Muthe, M. Kaur, A.K. Dua, S.C. Gadkari, S.K. Gupta, V.C. Sahni, Sens. Actuators B 96 (2003) 245–252.
[25] H.F. Helegourc, F. Arefi, R. Planade, J. Amouroux, Sens. Actuators B 73 (2001) 27–34.
[26] T. Maekawa, K. Suzuki, T. Takada, T. Kobayashi, M. Egashira, Sens. Actuators B 80 (2001) 51–58.
[27] B.T. Marquis, J.F. Vetelino, Sens. Actuators B 77 (2001) 100–110.
[28] R.K. Sharma, P.C.H. Chan, Z. Tang, G. Yan, I.M. Hsing, J.K.O. Sin, Sens. Actuators B 72 (2001) 160–166.
[29] N. Barsan, M. Schweizer, J. Anal. Chem. 365 (1999) 287–304.
[30] M. Egashira, M. Nskashima, J. Phys. Chem. 85 (1981) 4125–4130.
[31] D. Kohl, Sens. Actuators B 18 (1989) 71–113.
[32] V. Brinzari, G. Korotcenkov, Sens. Actuators B 98 (2004) 41–45.
[33] J. Zhu, Z. Lu, S.T. Aruna, D. Aurbach, A. Gedanken, Chem. Mater. 12 (2000) 2557–2566.
[34] S.C. Chang, Proceeding of International Meeting on Chemical Sensors, Furuoka, Japan, 1983, pp. 78–83.
[35] M.G. Fu, X.J. Wang, J. Zhengzhou Inst. Light Ind. 28 (1994) 160–166.
[36] S. Shukla, S. Seal, in: H.S. Nalwa (Ed.), Encyclopedia of Nanoscience and Nanotechnology, American Scientific Publisher, Stevenson Ranch, CA, USA, 2003.